Optics Letters

Simultaneous imaging of flow and sound using high-speed parallel phase-shifting interferometry

Kenji Ishikawa,[1,*] Risako Tanigawa,[1] Kohei Yatabe,[1] Yasuhiro Oikawa,[1] Takashi Onuma,[2] and Hayato Niwa[2]

[1]Department of Intermedia Art and Science, Waseda University, 3-4-1 Ohkubo, Shinjuku-ku, Tokyo 169-8555, Japan
[2]Photron Limited, 1-105 Kanda-Jinbocho, Chiyoda-ku, Tokyo 101-0051, Japan
*Corresponding author: k-ishikawa@fuji.waseda.jp

Received 13 December 2017; revised 11 January 2018; accepted 23 January 2018; posted 24 January 2018 (Doc. ID 315523); published 20 February 2018

In this Letter, simultaneous imaging of flow and sound by using parallel phase-shifting interferometry and a high-speed polarization camera is proposed. The proposed method enables the visualization of flow and sound simultaneously by using the following two factors: (i) injection of the gas, whose density is different from the surrounding air, makes the flow visible to interferometry, and (ii) time-directional processing is applied for extracting the small-amplitude sound wave from the high-speed flow video. An experiment with a frame rate of 42,000 frames per second for visualizing the flow and sound emitted from a whistle was conducted. By applying time-directional processing to the obtained video, both flow emitted from the slit of the whistle and a spherical sound wave of 8.7 kHz were successively captured.

OCIS codes: (110.3175) Interferometric imaging; (120.5050) Phase measurement; (120.5475) Pressure measurement.

https://doi.org/10.1364/OL.43.000991

Over the past decades, optical interferometry has been one of the most important measurement methods; it has been used for various applications in science and engineering. The progress in optical technologies has been expanding the applicable domain of interferometry. Particularly, the use of parallel phase-shifting interferometry (PPSI) [1,2] enables quantitative observation of dynamic phenomena such as vibration [3–5], gas flow [6,7], sound [8–10], electric discharge [11], and microscopic phenomena [12–14].

As interferometry is capable of measuring various phenomena, it is reasonable to consider measuring complex phenomena that involve the interaction of multiple physical processes. Simultaneous measurement of these processes can contribute to the understanding of the underlying physics of these complex phenomena. As properties of these processes are considerably different, special attention should be given to the measurement.

If we consider sound generation induced by flow, understanding the process and feedback mechanisms due to the interaction between flow and sound is crucially important in aeroacoustic problems. Modern aeroacoustics started with Lighthill's study [15]. Thus far, numerous studies have been dedicated to understanding the physical process in aeroacoustics [16] and reducing the noise caused by, e.g., high-speed trains [17] and wind turbines [18]. Generally, flow measurement is performed by using optical methods such as particle image velocimetry [19–21] and the Schlieren method [22–24], and sound is measured by a traversing microphone [25] or a microphone array [26,27] placed outside the flow field. Although far-field sound pressure can be measured, capturing the sound field inside of and near the flow is difficult. This prevents the direct observation of the interaction of flow and sound. Contrary to this, optical methods have been applied to measure sound [8–10,28–33], and these have the potential to achieve direct imaging of a sound field around flow due to their contactless nature. Nakazono *et al.* measured the intensity map of acoustic standing waves near a screeching jet, exhausting from a nozzle by using a scanning optical laser microphone [34]. The Schlieren method has been used for simultaneous imaging of flow and pressure waves, such as jet screech [35,36]. Until now, high-speed and simultaneous imaging of flow and sound in the audible range has not been achieved. As aeroacoustic problems in the audible range include aeroacoustic noise and aerophone sounds, which are critical to human hearing, the development of a simultaneous imaging method for those is required.

As PPSI has been used for the measurement of gas flow [6] and sound [8,9] independently, it is expected that PPSI can be applied to simultaneous aeroacoustic measurements. In fact, as its sensitivity does not depend on the frequency of sound, it is effective for measuring low-frequency sound. However, simultaneous measurement is difficult to achieve, due to the following: (i) in most cases, the flow-induced audible sound is caused by an incompressible air flow, and thus, such a flow is invisible to interferometry, and (ii) as variation in the optical phase caused by the audible sound is much smaller than 2π rad (typically, less than 0.5 rad for very powerful sounds), the sound cannot be recognized as the deformation of fringes of a period of 2π. Thus, to remove background phase orientation from

the obtained phase map and to emphasize the sound, post-processing is necessary.

In this Letter, we propose a gas injection method with time-directional processing for the simultaneous measurement of flow and sound, by using PPSI and a high-speed camera. A quantitative optical phase map can be obtained from measurement by PPSI. In order to observe the flow by PPSI, the gas, whose density is different from the surrounding air, is injected into the flow in place of the air. The gas causes the refractive index to change, and the flow is observed as a variation in the optical phase map. In order to recognize sound waves in the phase image, the background phase orientation has to be removed. As the background phase orientation exceeds 2π in most cases, it is required to unwrap the phase. For unwrapping of the phase image, two-dimensional methods are commonly used [37,38]. For the interferometric imaging of flow, as the phase contains fine patterns of the flow, the two-dimensional unwrapping becomes difficult. Considering that the measured data are presented as a high-speed video of the two-dimensional phase map, for the post-processing, we propose the use of a time-directional one-dimensional processing instead of a two-dimensional unwrapping. The time-directional processing is effective because both flow and sound are dynamic phenomena. The advantages of processing are avoiding the risk of failure of the unwrapping and the reduction in computational time for the unwrapping. By applying our two proposals, both flow and the audible sound can be captured; thus, the simultaneous imaging is achieved for aeroacoustic problems where sound is critical in the human hearing range. The following experiment was conducted to verify the feasibility of the proposed method.

In order to perform simultaneous and instantaneous imaging, a two-dimensional optical phase map has to be obtained by a single-shot at high speed. For this, PPSI [1,2] combined with a high-speed polarization camera [39] was used. Figure 1 illustrates the schematic of the experimental instruments. The optical system included a Fizeau-type polarized interferometer [40]. Note that any type of PPSI is acceptable for this application. Here, we chose the Fizeau type because it is less sensitive to sound-induced vibration of the optical components. A continuous-wave (CW) YAG laser with a wavelength of 532 nm and power of 70 mW was used as a light source. The distance between the reference plane and the mirror was 0.7 m. The quantitative phase map was calculated from the four phase-shifted interference fringes in a single image captured by a high-speed polarization camera (CRYSTA PI-1P developed by Photron Limited), the size of one pixel of which was 20 μm × 20 μm. This system detects the line integral of the refractive index along the optical path between the reference plane and the mirror.

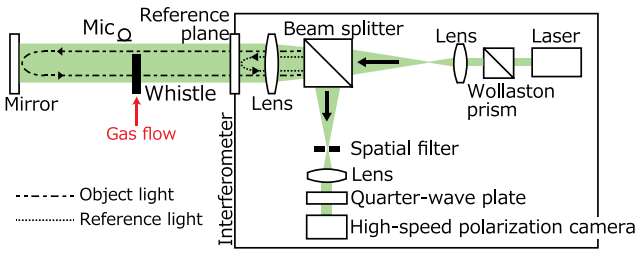

Fig. 1. Schematic of the experimental apparatus.

A whistle with resonant structure was chosen as a specimen of this experiment. The whistle is classified as an air-reed instrument, which generates sound by vibration of airflow. The mechanism of air-reed instruments has long been studied [41,42]; however, the physics of the underlying phenomena has not been completely understood. Thus, experimental observation of the dynamics of the flow and sound is important. The whistle was placed at the center of the optical path and at the bottom of the imaging area. For selecting the induced gas, molar mass is important because it affects the visibility of the flow. As the difference between the molar mass of the gas and the surrounding air increases, the change in optical phase increases. Therefore, one can adjust the visibility of the flow by changing the molar mass of the gas. In this experiment, 1,1-difluoroethane, with a molar mass of 66.05 g/mol, was used because it induces a sufficiently large change in the optical phase to visualize the gas flow in our case. The frame rate of the high-speed polarization camera was set to 42,000 frames per second, which was determined with respect to the frequency of the generated sound. The measurable area was 56 mm × 35 mm, and the pixel dimensions were 256 × 160. Figure 2 shows an example of the measured image to illustrate the position and the structure of the whistle. The whistle was positioned at the bottom of the imaging area, and its input port was on the right side. As interference fringes did not appear when the whistle intercepted the light, the position of the whistle could be distinguished from the other parts in the measured image. Both the flow and the sound were emitted from the slit near the edge of the whistle. The length of the cavity was approximately 7 mm, and its cross section was a circle. The sound was recorded by a microphone for reference. For calculating the phase values from the obtained pixel values of the camera, the hyper-ellipse fitting in the subspace method was used, because it can reduce the random noise and the phase-shifting error due to the imperfections of the optical components [43–45].

Figure 3(a) shows four successive obtained images. The periodical slanging lines are the phase discontinuities due to the wrap of phase. One period of the slanging lines corresponds to a phase variation of 2π. The gas flow emitted from the slit of the whistle is captured, while no sound appears on the images, because the phase variation caused by sound is much smaller than 2π. As the wrapped phase maps are largely distorted by the existence of the flow, the two-dimensional unwrapping develops a risk of failure. Instead of two-dimensional

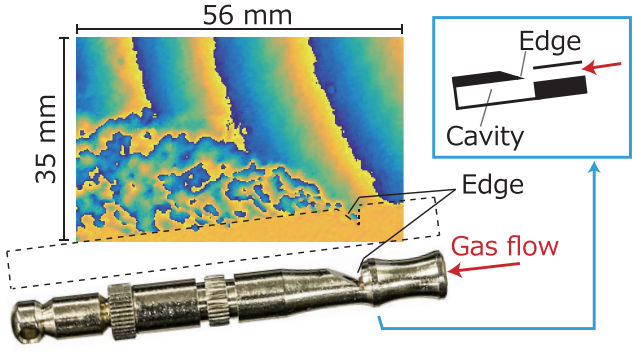

Fig. 2. Example of the measured image and the photo of the whistle. The whistle was located at the bottom of the imaging area. Its edge can be seen in the lower right of the image.

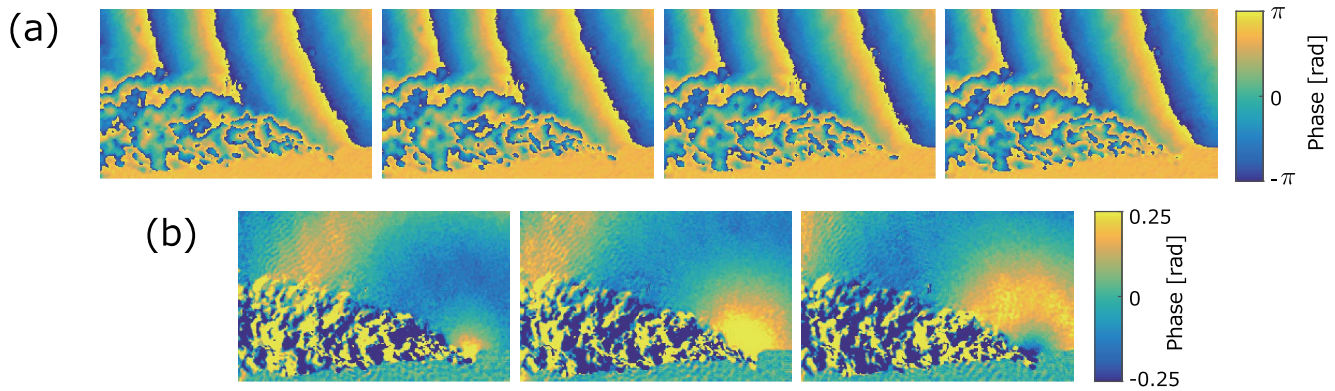

Fig. 3. Imaging results. (a) Phase images of four successive frames. (b) Differential images of the images in (a). The color range was chosen with respect to the amplitude of the sound wave (see Visualization 1).

unwrapping, we used the time-directional processing, which involves the following steps. First, the one-dimensional unwrapping to each pixel is performed, following which the values at each pixel of each time frame are subtracted by those of the next frame. This operation of taking the differences between two successive images corresponds to the temporal differential operation of the discrete signals. This operation can eliminate the background phase orientation, and can save time, compared to two-dimensional unwrapping for every frame. Furthermore, because the differential operation can be regarded as time-directional high-pass filtering, low-frequency components contained in the flow pattern are suppressed. Consequently, the differential operation can emphasize the sound and attenuate the flow. The differential images are shown in Fig. 3(b), and the corresponding movie is presented in Visualization 1. The range of the color was chosen with respect to the amplitude of the sound wave. The periodic slanging lines due to the background phase orientation are eliminated, and the spherical waveform, whose origin is near the slit of the whistle can be seen clearly. As shown in Visualization 1, the spherical wave propagates outward from the origin, and the flow propagates along the whistle. Moreover, it is clear from the movie that the spherical wave is much faster than the flow. In the next paragraph, we discuss whether the spherical pattern is a sound wave. In both Figs. 3(a) and 3(b), the flow is visualized as the translation and deformation of the specific patterns. The interferometric visualization of flow, as in Fig. 3(a), has been used for observing the characteristics of the flow field, such as velocity and vortex [46–48]. Thus, a similar analysis can be applied to the results of Fig. 3(a). For the flow in Fig. 3(b), the visualized patterns are related to the motion of the fluid particles because of the temporal differential operation. In both cases, pointwise quantitative values may be obtained by applying a holographic reconstruction technique [47] or a tomographic reconstruction technique [49].

In order to confirm that the obtained spherical pattern in Fig. 3(b) is the sound emitted from the whistle, the power spectra calculated from the PPSI and the microphone data are plotted in Fig. 4. The PPSI spectrum is calculated from the averaged values of 10 pixels × 10 pixels in the upper-right part of the images. Both spectra show two peaks at 8.7 kHz and 17.4 kHz. The difference in the lower frequency region arises from the difference in the noise characteristics of the instruments. The small peak at 15.9 kHz in the PPSI spectrum is due to the aliasing of the third-harmonic components. As the frequency of the third-harmonic components is 26.1 kHz and the sampling frequency of PPSI is 42 kHz, its aliased component appears at 15.9 kHz. This occurs because the high-speed camera does not have anti-aliasing filters. The audio files extracted from the microphone and PPSI data are given as Visualization 2. Since their lower-frequency regions differ, as can be seen in Fig. 4, we applied a high-pass filter, which eliminates frequency components less than 4000 Hz. Visualization 2 contains the four types of audio data: the microphone data, microphone data with filtering, PPSI data, and PPSI data with filtering. The duration of each type of audio data is 0.1 s. Whistling tones are audible in all of them. For the PPSI data without filtering, a low tone is heard. Both types of filtered data sound very similar. According to the above discussions, it can be said that the circular patterns in the images are the sound waves emitted from the whistle. Thus, PPSI successively measured the flow and the sound waves simultaneously.

Finally, in order to see the long-term trend of the phenomena, differential images with an interval of 200 frames are shown in Fig. 5, and a movie, which contains only one in every 10 frames of the images, is presented in Visualization 3. The origin of the time was set to coincide with the beginning of the flow emission. The temporal evolution of the gas flow is clearly visualized. The gas flow is emitted toward the upper-left then, and it gradually falls and propagates along the whistle. The sound appears approximately 30 ms after the beginning of the flow emission. It can be seen in the movie that the amplitude of sound gradually increases. This transient characteristic

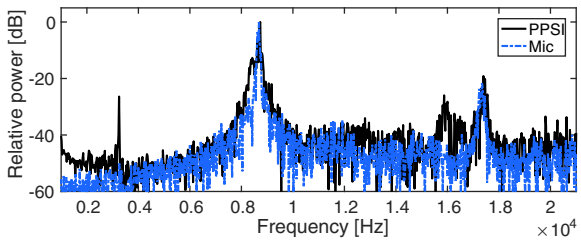

Fig. 4. Power spectrum of PPSI and microphone data. The PPSI spectrum was calculated from the averaged waveform of 10 pixels × 10 pixels in upper-right area in the images.

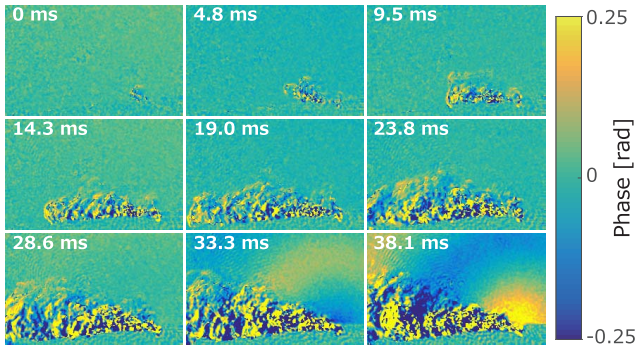

Fig. 5. Differential images with an interval of 4.76 ms, corresponding to 200 frames. The emission of the flow was begun at 0 ms. The sound wave appeared approximately after 30 ms (see Visualization 3).

represents the acoustic resonance in the whistle cavity induced by the gas flow. Furthermore, other characteristics of the phenomenon, such as the difference in propagation speeds and propagation manners of the flow and sound, also can be seen in the obtained movie.

In summary, we proposed a gas injection method with time-directional processing for the simultaneous measurement of flow and sound, by using PPSI and a high-speed camera. The gas was injected for the visualization of the incompressible air flow, and the time-directional processing was used to remove the background phase and to emphasize the sound. The experiment confirmed that the proposed method achieved simultaneous imaging of the flow and sound in the audible range. This method expands the field of experimental imaging for aeroacoustic problems to the audible sound range, application of which includes the investigation of aerophones and aeroacoustic noise caused by vehicles and machines [16–18]. The future direction of this research includes considering appropriate time-directional filters for the extraction of sound, quantitatively evaluating the flow field, and applying this method to various aeroacoustic problems. Furthermore, as the idea of using high-speed optical interferometry and time-directional processing can be applied to measure other complex physical phenomena, it can be applied to various domains, including acoustics, fluid dynamics, thermodynamics, and applied mechanics.

Funding. Japan Society for the Promotion of Science (JSPS); Grant-in-Aid for JSPS Research Fellow (16J06772); JSPS Grant-in-Aid for Research Activity Start-up (17H07191).

REFERENCES

1. Y. Awatsuji, M. Sasada, and T. Kubota, Appl. Phys. Lett. **85**, 1069 (2004).
2. J. E. Millerd, N. J. Brock, J. B. Hayes, M. B. North-Morris, M. Novak, and J. C. Wyant, Proc. SPIE **5531**, 304 (2004).
3. T. Kakue, Y. Endo, T. Nishitsuji, T. Shimobaba, N. Masuda, and T. Ito, Sci. Rep. **7**, 10413 (2017).
4. M. Ney, A. Safrani, and I. Abdulhlaim, J. Opt. **18**, 09LT02 (2016).
5. M. Ney, A. Safrani, and I. Abdulhalim, Opt. Lett. **42**, 719 (2017).
6. T. Kakue, R. Yonesaka, T. Tahara, Y. Awatsuji, K. Nishio, S. Ura, T. Kubota, and O. Matoba, Opt. Lett. **36**, 4131 (2011).
7. T. Fukuda, Y. Wang, P. Xia, Y. Awatsuji, T. Kakue, K. Nishio, and O. Matoba, Opt. Express **25**, 18066 (2017).
8. O. Matoba, H. Inokuchi, K. Nitta, and Y. Awatsuji, Opt. Lett. **39**, 6549 (2014).
9. K. Ishikawa, K. Yatabe, N. Chitanont, Y. Ikeda, Y. Oikawa, T. Onuma, H. Niwa, and M. Yoshii, Opt. Express **24**, 12922 (2016).
10. K. Ishikawa, K. Yatabe, Y. Ikeda, Y. Oikawa, T. Onuma, H. Niwa, and M. Yoshii, Proc. SPIE **10328**, 103280I (2017).
11. P. Xia, Y. Awatsuji, K. Nishio, and O. Matoba, Electron. Lett. **50**, 1693 (2014).
12. T. Tahara, K. Ito, T. Kakue, M. Fujii, Y. Shimozato, Y. Awatsuji, K. Nishio, S. Ura, T. Kubota, and O. Matoba, Biomed. Opt. Express **1**, 610 (2010).
13. A. Safrani and I. Abdulhalim, Appl. Opt. **54**, 5083 (2015).
14. A. Safrani and I. Abdulhalim, Opt. Lett. **40**, 4651 (2015).
15. M. J. Lighthill, Proc. R. Soc. London A **211**, 564 (1952).
16. P. J. Morris and G. M. Lilley, *Aerodynamic Noise: Theory and Applications* (Wiley, 2008), pp. 128–158.
17. C. Talotte, J. Sound Vib. **231**, 549 (2000).
18. S. Wagner, R. Bareiß, and G. Guidati, *Wind Turbine Noise* (Springer, 1996).
19. C. E. Willert and M. Gharib, Exp. Fluids **10**, 181 (1991).
20. R. J. Adrian, Exp. Fluids **39**, 159 (2005).
21. R. J. Adrian and J. Westerweel, *Particle Image Velocimetry* (Cambridge University, 2011).
22. G. S. Settles, *Schlieren and Shadowgraph Techniques* (Springer, 2001).
23. D. R. Jonassen, G. S. Settles, and M. D. Tronosky, Opt. Laser Eng. **44**, 190 (2006).
24. M. Raffel, Exp. Fluids **56**, 60 (2015).
25. J. Panda, J. Fluid Mech. **378**, 71 (1999).
26. J. I. Hileman, B. S. Thurow, E. J. Caraballo, and M. Samimy, J. Fluid Mech. **544**, 277 (2005).
27. A. Henning, K. Kaepernick, K. Ehrenfried, L. Koop, and A. Dillmann, Exp. Fluids **45**, 1073 (2008).
28. Y. Oikawa, Y. Ikeda, M. Goto, T. Takizawa, and Y. Yamasaki, in *Proceedings of IEEE International Conference on Acoustics, Speech, and Signal Processing* (IEEE, 2005), pp. 661–664.
29. A. Torras-Rosell, S. Barrera-Figueroa, and F. Jacobsen, J. Acoust. Soc. Am. **131**, 3786 (2012).
30. K. Bertling, J. Perchoux, T. Taimre, R. Malkin, D. Robert, A. D. Rakić, and T. Bosch, Opt. Express **22**, 30346 (2014).
31. T. Koukoulas and B. Piper, Appl. Phys. Lett. **106**, 164101 (2015).
32. K. Yatabe, K. Ishikawa, and Y. Oikawa, J. Sound Vib. **394**, 171 (2017).
33. N. Chitanont, K. Yatabe, K. Ishikawa, and Y. Oikawa, Appl. Acoust. **115**, 109 (2017).
34. Y. Nakazono, Y. Sonoda, Y. Ouchi, and Y. Nasu, J. Visualization **11**(2), 153 (2008).
35. G. Raman, J. Fluid Mech. **336**, 69 (1997).
36. G. Raman, J. Sound Vib. **225**, 543 (1999).
37. R. Goldstein, H. Zebker, and C. Werner, Radio Sci. **23**, 713 (1988).
38. D. C. Ghiglia and M. D. Pritt, *Two-Dimensional Phase Unwrapping: Theory, Algorithms and Software* (Wiley, 1998).
39. T. Onuma and Y. Otani, Opt. Commun. **315**, 69 (2014).
40. T. Yatagai, B. J. Jackin, A. Ono, K. Kiyohara, M. Noguchi, M. Yoshii, M. Kiyohara, H. Niwa, K. Ikuo, and T. Onuma, Proc. SPIE **9660**, 966018 (2015).
41. J. W. Coltman, Phys. Today **21**(11), 25 (1968).
42. M. S. Howe, J. Fluid Mech. **71**, 625 (1975).
43. K. Yatabe, K. Ishikawa, and Y. Oikawa, J. Opt. Soc. Am. A **34**, 87 (2017).
44. K. Yatabe, K. Ishikawa, and Y. Oikawa, Opt. Express **25**, 29401 (2017).
45. K. Yatabe, K. Ishikawa, and Y. Oikawa, Opt. Express **24**, 22881 (2016).
46. D. Watt and C. Vest, Exp. Fluids **5**, 401 (1987).
47. N. Andrés, P. Arroyo, and M. Quintanilla, Appl. Opt. **36**, 6997 (1997).
48. W. Sun, J. Zhao, J. Di, Q. Wang, and L. Wang, Opt. Express **17**, 20342 (2009).
49. D. Watt and C. Vest, Exp. Fluids **8**, 301 (1990).